Bonding and electronics of the $MoTe_2$/Ge interface under strain

Maciej J. Szary*
Institute of Physics, Poznan University of Technology, 62-965 Poznan, Poland

Marek T. Michalewicz
*A*STAR Computational Resource Centre, Singapore 138632, Singapore;*
Interdisciplinary Centre for Mathematical and Computational Modelling, ulica Kupiecka 32, 03-046 Warsaw, Poland;
and Institute for Advanced Computational Science, Stony Brook University, New York, USA

Marian W. Radny†
Institute of Physics, Poznan University of Technology, 62-965 Poznan, Poland
and School of Mathematical and Physical Sciences, The University of Newcastle, Callaghan 2308, Australia
(Received 19 November 2016; revised manuscript received 24 April 2017; published 17 May 2017)

Understanding the interface formation of a conventional semiconductor with a monolayer of transition-metal dichalcogenides provides a necessary platform for the anticipated applications of dichalcogenides in electronics and optoelectronics. We report here, based on the density functional theory, that under in-plane tensile strain, a 2H semiconducting phase of the molybdenum ditelluride ($MoTe_2$) monolayer undergoes a semiconductor-to-metal transition and in this form bonds covalently to bilayers of Ge stacked in the [111] crystal direction. This gives rise to the stable bonding configuration of the $MoTe_2$/Ge interface with the $\pm$K valley metallic, electronic interface states exclusively of a Mo 4*d* character. The atomically sharp Mo layer represents therefore an electrically active (conductive) subsurface δ-like two-dimensional profile that can exhibit a valley-Hall effect. Such system can develop into a key element of advanced semiconductor technology or a novel device concept.

DOI: 10.1103/PhysRevB.95.205421

I. INTRODUCTION

Since the discovery of graphene and surprises that emerged from exploring its low-dimensional physics, such as massless Dirac electrons or anomalous quantum Hall effect [1], the interest in other two-dimensional (2D) layered materials has grown rapidly [2–4]. Among them, exfoliated layers of transition-metal dichalcogenides (TMDs) have gained particular interest due to their intrinsic properties that are distinct from those of graphene. This includes the coexistence of *s*, *p*, and *d* electrons, absence of dangling bonds, inherent direct/indirect band gaps in semiconducting TMDs [4,5], and spin-split electronic bands due to inversion symmetry breaking [6]. Many features that are important in the realization of electronic or optoelectronic devices, such as electrostatics control or tunable optical properties, directly arise from such effects. On top of that, TMDs share important similarity with graphene—high elasticity with predicted strain resistance up to 20% [7]—adding further application perspectives.

A TMD monolayer consists of strongly bonded $X-M-X$ hexagonal layers, with M being a layer of transition-metal atoms of groups IV–VI (most common are Mo, Nb, W, Ta, and Ti) and X being a layer of chalcogen atoms (S, Se, or Te). Each M atom is coordinated by six nearest-neighbor X atoms in the trigonal prismatic geometry that breaks inversion symmetry of the monolayer. In bulk TMDs, the monolayers interact with each other by weak van der Waals (vdW) forces due to the lack of unsaturated (dangling) bonds on their surfaces. While the pristine surfaces of a TMD monolayer allow for engineering novel van der Waals heterostructures [8], they make it difficult to form strong interface bonds. The latter is important in electronics where the quality of (electrical) contacts within the device's circuitry controls the charge flow within the device and governs its overall performance. Typically, the pristine surface of TMDs interfaced with a metal increases the contact resistance and limits the charge transfer within the device [9]. Substitutional doping that is usually adopted in conventional semiconductors to reduce the contact resistance is not applicable in the 2D limit as it modifies the material and its properties. The latter also applies to TMDs with defects that are known to facilitate local electron transfer and covalent bond formation. The phase engineering approach, in which the octahedral 1T metallic phase was chemically modified to covalently functionalize TMD semiconductors, was demonstrated recently for $MoSe_2$, MoS_2, and VS_2 [10]. Phase engineering was proven to be particularly effective for $MoTe_2$ due to the small energy difference between the 2H phase and the metastable 1T′ phase for Mo- and W-based TMD monolayers. Other studies also predict that $MoTe_2$ monolayers undergo 2H-1T′ transitions induced by tensile strains [11,12], atoms and molecules adsorption [13], and electronic excitation [14]. The phase change from 2H to 1T′ in $MoTe_2$ induced by biaxial tensile strain up to 15% produces the 1T′ phase as a more stable structure; however, the activation barrier for this transition was calculated to be of 0.9 eV [12].

In this paper, we report the emergence of covalent bonding at the interface between a film of conventional semiconductor (Ge) and a $MoTe_2$ monolayer facilitated by strain applied to the monolayer in the 2H phase. The strain induces a semiconductor-to-metal transition in 2H-$MoTe_2$ and when such system is interfaced with bilayers of Ge stacked in the [111] crystal direction, it gives rise to the most stable atomic configuration of the $MoTe_2$/Ge interface. The *p*-type covalent

*Corresponding author: maciejjanszary@gmail.com
†Corresponding author: marian.radny@newcastle.edu.au

bonds at the interface result in seamless contact between the $MoTe_2$ monolayer and the Ge film. The system is metallic with the electronic states of a Mo 4*d* character crossing the Fermi level at the *K* points of the surface Brillouin zone (SBZ). The atomically sharp Mo layer represents, therefore, an electrically active δ-like 2D profile that can lead to a valley-Hall effect, which may significantly enrich the functionality of similar components present in conventional semiconductor-based electronics, such as in GaAs- and InP-based photonic devices [15].

II. METHODS

Total-energy and electronic structure calculations were performed based on the density functional theory as implemented in the QUANTUM ESPRESSO code [16]. The Projector augmented wave (PAW) potentials [17,18] and the kinetic-energy cutoff of 750 and 6800 eV for wave functions and densities, respectively, were used in the study. The vdW interaction was included and treated within a dispersion-corrected density functional theory (DFT-D) approach [19,20]. For exchange and correlation, the generalized gradient approximation–Perdew-Burke-Ernzerhof (GGA-PBEsol) functional was adopted [21,22]. The irreducible part of the surface Brillouin zone was sampled by a $12 \times 12 \times 1$ grid of *k* points generated using the Monkhorst-Pack scheme [23]. All calculations were performed in full-relativistic regime.

The systems were modeled by repeated asymmetric slabs that consist of up to seven bilayers of Ge subsequently stacked in the [111] crystal direction and interfaced with the $MoTe_2$ monolayer in three distinct interface configurations, shown in Fig. 2. The open surface of the Ge film was terminated by hydrogen atoms to prevent the electronic states at the interface from being contaminated by the states that might occur on this free surface (see Fig. 2). In the total-energy calculations, atomic positions were relaxed for all the atoms in the system with the adopted convergence threshold on forces (less than 10^{-5} Ry/a.u.). The separation between the slabs (vacuum) of 20 Å was found to be sufficient.

All of the calculations were performed with the relaxed lattice constant of bulk Ge equal to 5.658 Å, which for the $MoTe_2$ monolayer is equivalent to 14% homogeneous biaxial strain. Hence, in this approach, both systems share the same primitive hexagonal unit-cell equivalent to that of the Ge(111)-1×1 surface. Preliminary calculations for clean $MoTe_2$ conducted within 2×2 and 3×3 supercells under tensile strain exhibited no surface structural phase transitions. Similar calculations performed for strained $MoTe_2$ interfaced with one bilayer and six bilayers of Ge did not show any atomic reconstruction at the interface. Therefore, all of the reported calculations were performed within the 1×1 surface unit cell.

III. RESULTS

We first consider the structural and electronic properties of an isolated, strained $MoTe_2$ monolayer and compare them to those of the unstrained one. Upon relaxation within the Ge(111)-1×1 unit cell (see Sec. II), which is equivalent to 14% homogeneous biaxial strain, the atomic structure of $MoTe_2$ preserves its 2H phase. The calculations performed for the strained 2H phase of $MoTe_2$ within 2×2 and 3×3 supercells provide no evidence for any structural phase changes or deformations due to, for example, bond breaking or atom movement. The lack of the 2H to 1T′ transition in our calculations can be understood in the context of the results presented in Ref. [12], where the 2H-1T′ phase transition was identified to be due to simultaneous movement of the TM atom and Te atoms in their planes, associated with the activation barrier of ~ 0.9 eV. Structurally, the strained 2H phase of $MoTe_2$ is characterized by the increased Mo-Te bond lengths, from 2.71 to 2.82 Å, and the decreased Te-Mo-Te angles, from 82.9° to 70.8°, both resulting in the monolayer thickness reduced from 3.59 to 3.28 Å.

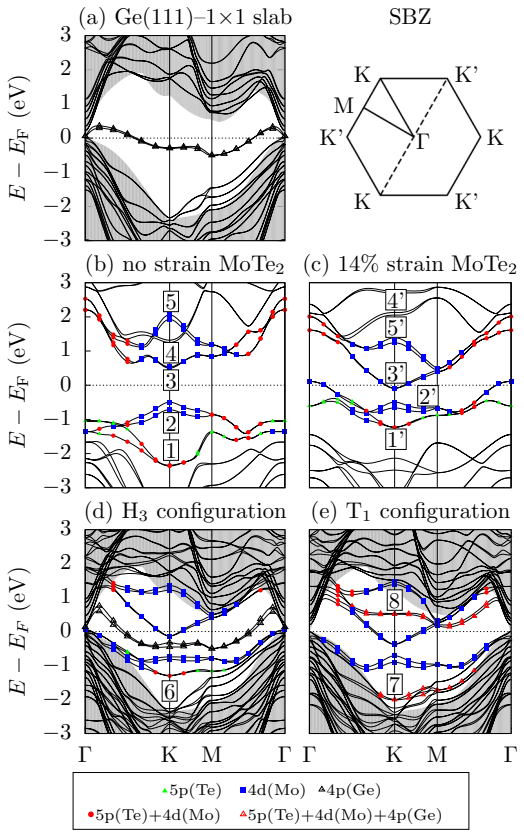

FIG. 1. Electronic band structures of (a) the isolated Ge(111) seven bilayers film (solid lines) with the bulk Ge band structure projected on the [111] direction (shaded area), (b) the isolated unstrained $MoTe_2$ monolayer, (c) the isolated strained $MoTe_2$ monolayer, (d) the $MoTe_2$/Ge interface in configuration H_3, and (e) the $MoTe_2$/Ge interface in configuration T_1. A schematic of SBZ with high symmetry points indicated is shown next to (a). The shaded area in (d) and (e) represents the bulk Ge band structure projected on the [111] direction.

These structural changes affect the electronic structure of the $MoTe_2$ monolayer, as shown in Fig. 1. The electronic band structure shown in Fig. 1(b) demonstrates that the unstrained monolayer is a direct-gap (1.05 eV) semiconductor with both the valence and conduction bands in the vicinity of the Fermi level (E_F) predominantly of the Te 5*p* and Mo 4*d* character (Te 5*s* states are localized at -12 eV and do not contribute to the bands near E_F). The valence and conduction bands' extrema are predominantly of the Mo $4d_{xy}/d_{x^2-y^2}$ and Mo d_{z^2} character [bands 2 and 3 in Fig. 1(b)], consistent with other reports [6].

TABLE I. Calculated binding energies of the H, Ge, Pb, and Si atoms on $MoTe_2$ adsorbed at three adsorption sites, T_1, T_4, and H_3 [these sites are equivalent to those of the $MoTe_2$ surface shown in Fig. 2].

	No strain			Strain		
Atom	H_3	T_1	T_4	H_3	T_1	T_4
	(eV)					
H	−1.66	−1.14	−1.08	−2.78	−2.41	−3.04
Ge	−0.66	−0.73	−0.42	−1.11	−1.38	−1.66
Pb	−0.62	−0.63	−0.52	−0.95	−1.17	−0.98
Si	−0.80	−0.86	−0.52	−1.32	−1.49	−1.96

As a result of inversion symmetry breaking, spin-orbit-induced spin splitting is observed in some of the bands with the largest splitting of 0.17 and 0.22 eV at the top of the valence band at the K point for strain and unstrain $MoTe_2$, respectively. This is also consistent with previous reports [6,24].

Under strain, the system undergoes a semiconductor-to-metal transition [see Fig. 1(c)] as a result of reduced dispersion of the Mo 4d bands. Similar electronic effects were reported in [14,25–27]. In particular, conduction band 3 at point K and valence band 2 in the Γ point, which are of the same Mo d_{z^2} character at these points, cross the Fermi level. These changes are consistent with the results of Johari and Shenoy [28], where the gap-size reduction and the transition from direct to indirect gap were reported for $MoTe_2$ under 10% strain. The dispersion of the band of predominantly Te $5p_z$ character at the K point [band 1 in Fig. 1(b)] is also reduced with its minimum at −2.0 eV (point K) shifted up in energy to −1.0 eV [band 1′ in Fig. 1(c)].

The impact of strain on the chemical activity of $MoTe_2$ is demonstrated first by calculating the binding energy of the H, Si, Pb, and Ge atoms adsorbed on the monolayer (see Table I). The binding energy was calculated as a total energy of the system upon adsorption (at three possible adsorption sites) minus the sum of the energies of the isolated components calculated in equivalent unit cells. The calculations were performed in the nonrelativistic regime with the vdW correction (DFT-D) included.

The data in Table I shows that for the equilibrium bonding configuration, the values of the adatoms binding energies calculated for $MoTe_2$ under strain are, on average, two times higher than the ones obtained for the unstrained $MoTe_2$ sample. This indicates that $MoTe_2$ under strain forms strong chemical bonds with the adatoms. The Lödwin charge analysis presented in Table II shows that isolated $MoTe_2$ under 14% strain exhibits a net charge transfer of 0.13e from Mo to Te when compared to the unstrained monolayer. The same trend is observed for the $MoTe_2$/adatom systems (Ge in Table II). These observations are in line with recently reported strain-induced charge excess around dichalcogen atoms (and the consequent depletion around transition-metal atoms) for MoS_2 and WS_2 [30]. Our data also shows that negative charge is accumulated on the dichalcogen atoms and the adatom (Ge in Table II), which illustrates that the strained TMD surface favors the formation of strong chemical (covalent) bonds. This results in higher adatom binding energies (see Table I).

TABLE II. Atom and l-resolved Lödwin charge distribution [29] (in $-e$) calculated within the unstrained and strained isolated $MoTe_2$ monolayer and the corresponding $MoTe_2$/Ge adsorption system.

			Partial charge		
	Atom	Total charge	s	p	d
		No strain			
	Te	15.33	1.57	3.77	10.00
	Mo	15.11	2.42	7.12	5.57
	Te	15.33	1.57	3.77	10.00
$MoTe_2$		Strain			
	Te	15.42	1.60	3.81	10.00
	Mo	14.98	2.51	7.14	5.33
	Te	15.42	1.60	3.81	10.00
		No strain			
	Ge	14.10	1.87	2.23	10.00
	Te	15.15	1.49	3.67	10.00
	Mo	15.13	2.42	7.12	5.60
	Te	15.33	1.57	3.77	10.00
T_1		Strain			
	Ge	15.04	1.90	2.14	10.00
	Te	15.25	1.52	3.74	10.00
	Mo	15.05	2.51	7.14	5.40
	Te	15.42	1.60	3.82	10.00

The $MoTe_2$/Ge interface formation was investigated by subsequent adsorption of Ge bilayers (germanene) on strained (14%) $MoTe_2$. The Te layers of the $MoTe_2$ monolayer under 14% strain have the hexagonal unit cells equivalent to that of the surface of a Ge(111)-1 × 1 film so the adsorbed bilayers of Ge are in their equilibrium atomic configurations. The subsequent adsorption of such bilayers results in the formation of the multilayered Ge(111) film interfaced with $MoTe_2$.

The interface configurations under study are schematically shown in Fig. 2 with strained $MoTe_2$ interfaced with the Ge(111) film of six bilayers of Ge. In the H_3 and T_4 geometries,

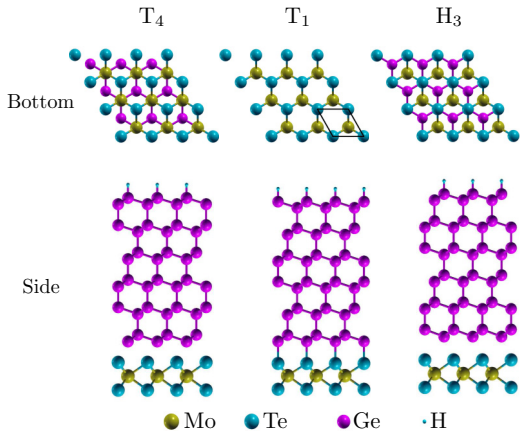

FIG. 2. Schematics of atomic structures (bottom and side views) of $MoTe_2$/Ge(111) interfaces in configuration H_3, T_1, and T_4. The surface unit cell, equivalent to that for Ge(111)-1 × 1, is shown in configuration T_1. The bottom view presents $MoTe_2$ and the first bilayer of the Ge film.

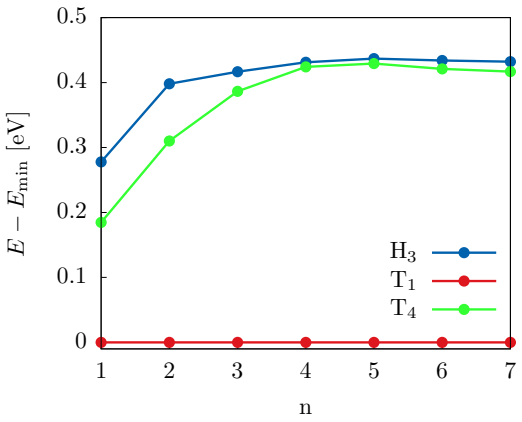

FIG. 3. Relative energetics of the $MoTe_2$/Ge interfaces as a function of a number of bilayers (n) in the Ge film. The reference energy is that of configuration T_1.

each bottom-most Ge adatom is located at the hollow site of the Te atomic layer and interacts with three top Te atoms. The difference between these geometries is that in T_4, the bottom-most Ge adatoms are located above the Mo atoms, while in H_3, the Ge adatoms are placed at the hollow sites of the $MoTe_2$ monolayer (at the center of honeycomb hexagons). In configuration T_1, the Ge atoms are placed directly above the top-layer Te atoms and each Ge interacts with one Te atom.

The calculated energetics of the systems is shown in Fig. 3. Geometry T_1 was found to be the most stable independently of the number of Ge bilayers interfaced with $MoTe_2$. The interface configuration with one bilayer of Ge is lower in energy by 0.18 and 0.28 eV than the corresponding H_3 and T_4 structures, respectively. Interestingly, the adsorption of more bilayers of Ge makes the $MoTe_2$/Ge interface more stable—the data in Fig. 3 shows that the energy separation between T_1, and T_4/H_3 increases to 0.42 eV and remains unchanged for the films with four or more bilayers of Ge. Inclusion of the van der Waals (vdW) interactions preserves this energetic order with the energy separation between T_1 and T_4 remaining at 0.4 eV. However, the vdW corrections clearly separate configurations T_4 and H_3, with the latter being ~ 0.1 eV lower in energy for the films with four or more bilayers of Ge. The dependence of the energetic stability on the number of bilayers of Ge in the $MoTe_2$/Ge interfaces is also reflected in the geometries of the systems (see Table III). In the most stable configuration, T_1, the Te-Ge bond length of 2.84 Å for one Ge bilayer is reduced to 2.67 Å for seven bilayers. In the T_4/H_3 geometries, the Te-Ge distances of 4.05 Å (H_3) and 3.68 Å (T_4) for one bilayer of Ge are reduced to 3.53 Å (H_3) and 3.44 Å (T_4) for seven bilayers.

The observed significant difference in the structural parameters between the T_4/H_3 and T_1 interface configurations indicates a different type of bonding in these structures. The nature of bonding at the $MoTe_2$/Ge interfaces is revealed in the electronic structures calculated for geometries H_3 [Fig. 1(d)] and T_1 [Fig. 1(e)] with seven bilayers of Ge (the structure for configuration T_4 is very similar to that for H_3 and is not shown). The electronic band structure of the $MoTe_2$/Ge interface with seven bilayers of Ge develops to the one that can be presented within the bulk Ge band structure projected on the reciprocal

TABLE III. Calculated bond lengths and interlayer spacings (in brackets) of the $MoTe_2$/Ge(111) interface in configurations H_3, T_1, and T_4. The corresponding data for the isolated Ge slab and $MoTe_2$ monolayer are given in the first column (Ref.). Atoms are numbered from the bottom of the monolayer to the top of the Ge slab (see Fig. 2).

Bilayers	Atoms	Ref.	H_3	T_1	T_4
			(Å)		
1	Ge(1)-Ge(2)	2.46	2.41	2.45	2.41
		(0.83)	(0.67)	(0.81)	(0.69)
	Te(2)-Ge(1)		4.05	2.84	3.68
			(3.32)	(2.84)	(2.87)
	Mo-Te(2)	2.71	2.83	2.81	2.83
		(1.64)	(1.64)	(1.60)	(1.63)
	Te(1)-Mo	2.71	2.83	2.82	2.82
		(1.64)	(1.63)	(1.62)	(1.62)
7	Ge(2)-Ge(3)	2.46	2.46	2.47	2.47
		(2.46)	(2.46)	(2.47)	(2.47)
	Ge(1)-Ge(2)	2.46	2.49	2.45	2.46
		(0.83)	(0.92)	(0.8)	(0.85)
	Te(2)-Ge(1)		3.53	2.67	3.44
			(2.66)	(2.67)	(2.55)
	Mo-Te(2)	2.71	2.83	2.74	2.83
		(1.64)	(1.64)	(1.48)	(1.63)
	Te(1)-Mo	2.71	2.83	2.82	2.82
		(1.64)	(1.63)	(1.62)	(1.62)

space [111] direction [shaded areas in Figs. 1(e) and 1(f)]. In this scheme, the electronic structure of an isolated Ge film [Fig. 1(a)] has a metallic surface band located in the bulk Ge energy gap. This band is of a Ge $4p_z$ character and originates from the unsaturated, dangling bonds on the Ge(111)-1 × 1 surface of the film.

The electronic structure of configuration H_3 [Fig. 1(d)] is a simple combination of the band structure of the strained, isolated $MoTe_2$ monolayer [Fig. 1(c)] and the Ge slab [Fig. 1(a)] with the dispersion of the bands and their atomic characters preserved. By contrast, in the electronic structure of configuration T_1 [Fig. 1(e)], the bands of the Mo $4d$ character in the vicinity of E_F remain intact, but the Te $5p$ states [band 1' in Fig. 1(c)] and the Ge $4p$ states [metallic band in Fig. 1(a)] interact, resulting in the formation of two new bands, 8 and 7, in Fig. 1(e).

The origin of these new bands is resolved by inspecting the partial (pseudo-)charge density distribution for band 7 and the probability density distribution for band 8 calculated at the K point, are shown in Fig. 4. A significant bonding charge

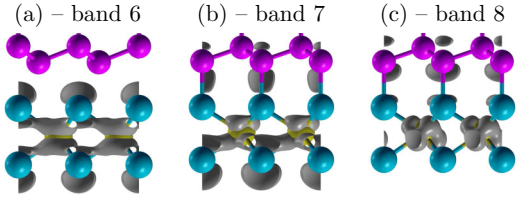

FIG. 4. Partial (pseudo-)charge densities ($|\psi|^2$) calculated for the states at point K for bands (a) 6, (b) 7, and (c) 8 in Figs. 1(d) and 1(e). Isosurface value: $0.0025e$/a.u.^{3}.

can be seen midway along the Te-Ge bonds for band 7 in Fig. 4(b), which corresponds to covalent bonds resulting from the bonding combination of the Te $5p_z$ and Ge $4p_z$ states. By contrast, the probability density for unoccupied band 8 [Fig. 4(c)] is significant only around the Te and Ge atoms with a nodal plane within the Te-Ge bond; this is a result of the antibonding combination of the Te $5p_z$ and Ge $4p_z$ states. Figure 4(a) shows that the charge distribution calculated at point K for band 6 in Fig. 1(d) for configuration H_3 is mirror symmetric with respect to the Mo layer, indicating that there is no influence of the Ge layer on the $MoTe_2$ states in this geometry. This is also equivalent to the charge distribution calculated for band 1 in Fig. 1(c) for the isolated monolayer.

The presented results are intriguing for a number of reasons. First, the calculated Te-Ge covalent bond of 2.7 Å at the MoTe2/Ge interface with seven bilayers of Ge in the most stable interface geometry, T_1, is significantly shorter than those found in the GeTe compounds (2.85–3.25 Å) [31]. As the covalency of the Ge-Te bonds is considered to be greater for the shorter bonds [32], our results suggest very strong covalent bonding at the $MoTe_2$/Ge interface. The data on Fig. 3 also show that the adsorption of just a single bilayer of Ge atoms on the 14% strained $MoTe_2$ monolayer produces the T_1 configuration as the most stable structure, with the adsorption of more layers of Ge making the covalent bonds at the interface even stronger. As the TMD monolayers are predicted to withstand 10–20% strain and Te atoms are known surfactants for the epitaxial growth of thick, low-defect Ge layers on Si, the epitaxial growth of Ge layers on the strained $MoTe_2$ monolayer, while challenging, may be a feasible task.

Second, both the isolated, strained $MoTe_2$ monolayer and the $MoTe_2$/Ge interface are metallic due to the electronic states at E_F of the Mo $4d_{z^2}$ character. However, the interface formation transfers the monolayer's conduction- and valence-band extrema localized interface states, as they are located in the (bulk) energy gap of the Ge film [see Figs. 1(d) and 1(e)]. Therefore, the Mo atoms are located beneath the open surface of the interface (Te) and are confined to a single atomic plane; they form the subsurface, conductive δ-like 2D profile. In addition to that, the Fermi level of the interface is located such that the Mo $4d_{z^2}$ states cross E_F exclusively at the K points of the surface Brillouin zone [SBZ; see Fig. 1(e) and the inset in Fig. 1]. However, the K points in the SBZ are not equivalent, and the equivalent pairs (K, K) or (K', K') are separated by a large distance in the momentum (k) space. The separation is such that when an electric field is applied to the system, the charge may flow in opposite directions, giving rise to the so-called valley-Hall effect (similar results can be obtained by exposing the interface to a circularly polarized light). While the quantitative accounts of these effects involve the calculations and analysis of a Berry curvature [6,33] and are outside the scope of this paper, the reported results highlight some intriguing consequences of a semiconductor-dichalcogenide interface formation on the electronic and optical properties of the formed systems.

IV. CONCLUSIONS

So far, mechanical strain has been shown to be an effective way to induce and tune the band gaps and structural phase transitions in TMD monolayer materials. Our density functional theory study reveals a surprising occurrence of strong covalent bonding at the strained 2H-$MoTe_2$/Ge interface and the formation of an atomically sharp δ-like 2D profile with conductive d electrons. The latter arises from the interaction of the Mo $4d$ orbitals in the strained $MoTe_2$ monolayer not affected by the interface formation with Ge. The results suggest a way for utilizing the strain-induced chemical activity of the TMD materials, d-electron physics, and valley electronics of dichalcogenides, and may evolve to develop novel electronic materials with unique applications.

ACKNOWLEDGMENTS

A*STAR Computational Resource Centre, Singapore, is acknowledged for access to the high-performance computing facilities. M.W.R. acknowledges the Polish Ministry of Science and Higher Education for support (Grant No. 06/62/DSPB/2173).

[1] K. S. Novoselov, D. Jiang, F. Schedin, T. J. Booth, V. V. Khotkevich, S. V. Morozov, and A. K. Geim, Proc. Nat. Acad. Sci. USA **102**, 10451 (2005).
[2] B. Aufray, A. Kara, S. Vizzini, H. Oughaddou, C. Léandri, B. Ealet, and G. Le Lay, Appl. Phys. Lett. **96**, 183102 (2010).
[3] M. E. Dàvila, L. Xian, S. Cahangirov, A. Rubio, and G. L. Lay, New J. Phys. **16**, 095002 (2014).
[4] K. F. Mak, C. Lee, J. Hone, J. Shan, and T. F. Heinz, Phys. Rev. Lett. **105**, 136805 (2010).
[5] A. Splendiani, L. Sun, Y. Zhang, T. Li, J. Kim, C.-Y. Chim, G. Galli, and F. Wang, Nano Lett. **10**, 1271 (2010).
[6] G.-B. Liu, W.-Y. Shan, Y. Yao, W. Yao, and D. Xiao, Phys. Rev. B **88**, 085433 (2013).
[7] R. C. Cooper, C. Lee, C. A. Marianetti, X. Wei, J. Hone, and J. W. Kysar, Phys. Rev. B **87**, 035423 (2013).
[8] A. K. Geim and I. V. Grigorieva, Nature (London) **499**, 419 (2013).
[9] A. Allain, J. Kang, K. Banerjee, and A. Kis, Nat. Mater. **14**, 1195 (2015).
[10] D. Voiry, A. Goswami, R. Kappera, S. d. C. C. e, D. Kaplan, T. Fujita, M. Chen, T. Asefa, and M. Chhowalla, Nat. Chem. **7**, 45 (2015).
[11] K.-A. N. Duerloo, Y. Li, and E. J. Reed, Nat. Commun. **5**, 4214 (2014).
[12] H. H. Huang, X. Fan, D. J. Singh, H. Chen, Q. Jiang, and W. T. Zheng, Phys. Chem. Chem. Phys. **18**, 4086 (2016).
[13] Y. Zhou and E. J. Reed, J. Phys. Chem. C **119**, 21674 (2015).
[14] A. V. Kolobov, P. Fons, and J. Tominaga, Phys. Rev. B **94**, 094114 (2016).
[15] J. J. Harris, J. Mater. Sci.: Mater. Electron. **4**, 93 (1993).

[16] P. Giannozzi, S. Baroni, N. Bonini, M. Calandra, R. Car, C. Cavazzoni, D. Ceresoli, G. L. Chiarotti, M. Cococcioni, I. Dabo, A. Dal Corso, S. de Gironcoli, S. Fabris, G. Fratesi, R. Gebauer, U. Gerstmann, C. Gougoussis, A. Kokalj, M. Lazzeri, L. Martin-Samos, N. Marzari, F. Mauri, R. Mazzarello, S. Paolini, A. Pasquarello, L. Paulatto, C. Sbraccia, S. Scandolo, G. Sclauzero, A. P. Seitsonen, A. Smogunov, P. Umari, and R. M. Wentzcovitch, J. Phys. Condens. Matter **21**, 395502 (2009).
[17] P. E. Blöchl, Phys. Rev. B **50**, 17953 (1994).
[18] G. Kresse and D. Joubert, Phys. Rev. B **59**, 1758 (1999).
[19] S. Grimme, J. Comput. Chem. **27**, 1787 (2006).
[20] V. Barone, M. Casarin, D. Forrer, M. Pavone, M. Sambi, and A. Vittadini, J. Comput. Chem. **30**, 934 (2009).
[21] J. P. Perdew, K. Burke, and M. Ernzerhof, Phys. Rev. Lett. **77**, 3865 (1996).
[22] J. P. Perdew, A. Ruzsinszky, G. I. Csonka, O. A. Vydrov, G. E. Scuseria, L. A. Constantin, X. Zhou, and K. Burke, Phys. Rev. Lett. **100**, 136406 (2008).
[23] H. J. Monkhorst and J. D. Pack, Phys. Rev. B **13**, 5188 (1976).
[24] Y. C. Cheng, Z. Y. Zhu, M. Tahir, and U. Schwingenschlögl, Europhys. Lett. **102**, 57001 (2013).
[25] S. Song, D. H. Keum, S. Cho, D. Perello, Y. Kim, and Y. H. Lee, Nano Lett. **16**, 188 (2016).
[26] S. Bhattacharyya and A. K. Singh, Phys. Rev. B **86**, 075454 (2012).
[27] W. S. Yun, S. W. Han, S. C. Hong, I. G. Kim, and J. D. Lee, Phys. Rev. B **85**, 033305 (2012).
[28] P. Johari and V. B. Shenoy, ACS Nano **6**, 5449 (2012).
[29] D. Sanchez-Portal, E. Artacho, and J. M. Soler, Solid State Commun. **95**, 685 (1995).
[30] M. Ghorbani-Asl, S. Borini, A. Kuc, and T. Heine, Phys. Rev. B **87**, 235434 (2013).
[31] J. L. F. Da Silva, A. Walsh, and H. Lee, Phys. Rev. B **78**, 224111 (2008).
[32] A. Kolobov, M. Krbal, P. Fons, J. Tominaga, and T. Uruga, Nat. Chem. **3**, 311 (2011).
[33] W. Feng, Y. Yao, W. Zhu, J. Zhou, W. Yao, and D. Xiao, Phys. Rev. B **86**, 165108 (2012).